High mass loading additive-free LiFePO4 cathodes with 500 μm thickness for high areal capacity Li-ion batteries

Carmen de La Torre-Gamarra, María Eugenia Sotomayor, Jean-Yves Sanchez, Belén Levenfeld, Alejandro Várez, Barbara Laïk, Jean Pierre Pereira-Ramos

High mass loading additive-free LiFePO4 cathodes with 500 μm thickness for high areal capacity Li-ion batteries

Carmen de la Torre-Gamarra[a], María Eugenia Sotomayor[a], Jean-Yves Sanchez[a,b], Belén Levenfeld[a], Alejandro Várez[a,*], Barbara Läik[c], Jean-Pierre Pereira-Ramos[c]

[a]*Departamento de Ciencia e Ingeniería de Materiales e Ingeniería Química, Universidad Carlos III de Madrid, Avda. Universidad 30, 28911, Leganés, Spain*
[b]*CNRS, Grenoble INP, LEPMI, Université Grenoble Alpes, Université Savoie Mont Blanc, UMR 5279, 38000, Grenoble, France*
[c]*CNRS, UMR 7182, Institut de Chimie et des Matériaux Paris Est, GESMAT, UPEC, Université Paris Est, 2 Rue Henri Dunant, F-94320, Thiais, France*

Abstract

We report the preparation of thick ceramic electrodes of the olivine $LiFePO_4$ (LFP) with high mass loading is reported. These electrodes are prepared by means of Powder Extrusion Moulding (PEM), which is a technology easily scalable and cheap. These LFP cathodes are additive-free (neither binder nor extra carbon black) with ~0.5 mm thickness, allowing to develop very high areal capacity (13.7 mA h cm^{-2}). By means of a strict control of sintering process, the carbon coating of the commercial LFP powder remains and the decomposition of the active material is prevented. The optimized self-supported LFP cathode presents good cyclability over 20 cycles at C/10 with no capacity loss. The good electrochemical performance of these novel LFP thick electrodes and their non-flammability make them interesting candidates for both mobile and stationary applications.

Keywords: thick electrode, binder-free, solvent-free, areal capacity, high mass loading

* Corresponding author

1. Introduction

Since the first proposal of $LiCoO_2$ as lithium intercalation material for Li-ion batteries (LIBs) by J.B. Goodenough in 1980 [1] and its commercialization by Sony in the early 1990s, LIBs have become an excellent technology for energy storage due to their high energy density, long cycle life and zero greenhouse gases emission. They are nowadays the most commonly used for power generation in portable devices and important developments have been achieved in terms of safety, cost and lifetime during the last years. Currently, LIBs are a key element in the development and implementation of the electric vehicle (EV) and the plug-in hybrid electric vehicle (PHEV). In the early future they will also be essential for the storage of electricity produced by intermittent renewable energy sources such as wind and sun [2]. However, in order to meet the requirements of electric transportation and of electricity storage high capacity LiBs still require great efforts. Indeed, they must overcome several current challenges in terms of energy density, lifetime, cost and above all safety. Thus, cost reductions regarding cathodes have motived the search of alternatives to lithium cobalt oxide, moving from Co to widespread and must cheaper elements such as Fe or Mn. The non-active components (electrolyte, binders, separators and current collectors) represent about half of the weight of the total battery and, therefore, also deserve to be considered in order to reduce significantly the battery cost. On the other hand, safety is a main concern for electromotive applications, so cathode materials that could prevent thermal runaway are desired [3].

Due to its fairly low cost and environmentally benignity (low toxicity) $LiFePO_4$ (LFP) is, among the commercial cathode materials, an interesting option for large-scale applications. LFP has a high structural stability, long lifetime, high power density and can undergo charges and discharges at very high rates. It must be also underlined that LFP working voltage is within the electrochemical stability window of commercial electrolytes, which minimizes the decomposition of typical liquid electrolytes [4]. Eventually, it is considered the safest cathode material, presenting a very high thermal stability and preventing O_2 evolution and thermal

runaway. Owing to its redox potential (3.4 V vs Li/Li^+), a variety of solvents and salts have the sufficient anodic stability to be used with LFP. Moreover, at this potential, salts safer than $LiPF_6$ as $LiCF_3SO_3$ and LiTFSI do not corrode the aluminum current collectors while positives operating at higher voltage, as $LiCoO_2$ or LNMC, require fluorinated solvents to passivate Al. Indeed, the main disadvantage of LFP lies in its lesser energy density compared with other cathode materials. This is not due to its practical specific capacity (~165 mA h g^{-1}), among the highest ones, but to its average potential (3.4 V) [5]. Currently, experimental and commercial LFP cathodes offer specific capacities close to the theoretical one and the working voltage is also very similar to the expected one. Therefore, no longer improvements can be achieved. On the other hand, in commercial batteries, volumetric and areal capacities are governed by the presence of non-active additives in the cathode, such as binders (PVDF or PTFE) and carbon (acetylene black or carbon black) [5]. Therefore, the minimization of the additives would lead to a rise in the areal capacity by increasing the active material mass per surface unit. In this sense, the concept of thick electrodes has been previously developed by deposition of active material on different substrates (e.g. metal foams, [6] textiles [7] and foils [8]). Nevertheless, in all these cases, the addition of a large amount of binder (~ 10-12 wt. %) is required. The limit of this approach would lead to the concept of additive-free or monolithic electrodes. On one hand, using thicker electrodes presents several advantages in terms of cost-cutting by reducing the assembly time (reduces the number of steps and avoids cutting or punching and cleaning afterwards), the surface areas of current collectors and separator, as well as the amount of costly and flammable electrolytes [9]. On the other hand, there is currently a worldwide motivation to develop All-Solid-State Batteries (ASSB) to achieve high power and energy densities compared to conventional LIBs while improving the battery safety. The combination of additive-free thick electrodes with a solid electrolyte paves the way to highly safe Li-ion batteries [10].

In this contribution, we propose the use of Powder Extrusion Moulding (PEM) technology for the manufacturing of additive-free thick LFP/C electrodes (~ 0.5 mm) with remarkable electrochemical performances. This technology is quite similar to Powder Injection Moulding and we successfully applied it to the manufacturing of microtubes and layers of YSZ, [11] Ni-YSZ [12,13] and ferritic stainless steels [14] for being used in self-supported, anode-supported and metal-supported solid oxide fuel cells (SOFCs), respectively. Recently we obtained, by this technology, thick ceramic electrodes of LTO with areal and volumetric capacities [15] as high as 15.2 mAh cm^{-2} and 319 mA h cm^{-3} at C/24 respectively. These additive-free ceramic electrodes present two remarkable advantages: non-flammability and ability to operate over a wider temperature range, without degradation or loss of integrity (two of the major concerns in the application of LIBs, especially for commercialization of EV and PHEV [16]), and the characteristic of being self-supported. Additionally, they result in a high amount of active material, increasing the electrochemical performances, namely the areal capacity. In this context, some recent studies reported the preparation of thick electrodes in which remarkable large areal capacities are reached [17,18,19]. Furthermore we have assembled a LIB composed of thick ceramic LTO and LFP additive-free electrodes [20] with a mass loading of ~100 mg cm−2 and areal capacity of 13.3 mA h cm^{-2}, allowing to deliver very high energy (about 23.9 mW h cm^{-2}). In this paper, we present details of the preparation process of the electrodes and also a systematic study of the electrochemical performance of sintered LFP electrodes. Analyzing the influence of the processing and the thickness of the sample, the effect of the electrolyte viscosity, the sintering temperature and the cut-off voltage on the electrodes capacity.

2. Experimental

2.1. Material preparation

LFP/C cathodes were prepared by using a commercial $LiFePO_4$/C powder (Linyi Gelon Lib Co. LTD), with a carbon content of (1.70 ± 0.01) wt. %, measured by elemental analysis (LECO CS-200 instrument), and a pycnometric density (Micrometrics AccuPyc 1330) of (3.57 ± 0.01) g cm^{-3}. The particle size distribution of the powder was determined by employing a Malvern Mastersizer 2000 instrument (see supplementary information- Fig. S1).

For the preparation of the ceramic LFP/C extruded electrode, Powder Extrusion Moulding (PEM) technology was employed. It consists in the following steps: (1) mixture of the powder with a polymeric binder system to produce a homogeneous mixture called feedstock, (2) extrusion of the feedstock to get the as-called green material, (3) debinding to remove the polymeric system by thermal treatment in a controlled atmosphere and eventually (4) sintering the material to obtain the final electrode. Thus, a binder system consisting on polypropylene (PP), paraffin wax (PW) and stearic acid (SA) in a volume ratio 50/46/4 was selected according to previous successful works on YSZ [11] and LTO [15]. The binder and the powder were firstly mixed for 40 minutes at 180 °C in a Haake Rheocord 252p mixer with a pair of rotor blades. To optimize the powder loading of the feedstock six different binder/powder formulations were prepared (volume ratios: 50/50, 49/51, 47.5/52.5, 45/55, 43.5/56.5 and 42/58).

The rheological characterization of some mixtures was performed in a capillary rheometer (Haake Rheocap) in a range of shear rates from 100 to 10000 s^{-1} and at temperatures between 160 and 190 °C. The measurements were developed with a temperature control of ± 1 °C. The dimensions of the die were 30 mm in length (L) and 1mm in diameter (D) in order to keep a constant L/D ratio of 30.

A Haake Rheomex CTW100p twin screw extruder was used to produce enough amount of the optimum formulation mixture. The mixture was extruded three times to get a homogeneous feedstock. Afterwards, the feedstock was granulated and vertically extruded in a single-screw extruder with a home-designed nozzle of 0.5 mm thickness and 6 mm width to obtain the so-called green parts with layer shape. The temperature profile of the barrel was optimized at 175/178/182/185 °C.

A combination of solvent and thermal debinding was used for removing the organic

component from the extruded pieces. Firstly, the green parts were immersed in n-heptane and subsequently, a thermal cycle was applied. Thermo Gravimetric Analysis (TGA) was performed in order to design the debinding thermal cycle using a Perkin Elmer TGA Pyris1 analyzer with N2 as working atmosphere from 30 to 900 °C with a heating rate of 10 °C min-1. Finally, sintering was carried out for 2 h at different temperatures (550, 600, 650, 750, 850 and 900 °C). Both thermal debinding and sintering were performed under inert N_2 atmosphere to prevent iron and carbon oxidation. The carbon content was measured after the different steps to ensure no carbon loss.

2.2 Material characterization

X-Ray Diffraction (XRD) patterns were recorded on a Philips X'Pert diffractometer equipped with a Cu-Kα radiation source. This instrument had (θ/2θ) Bragg–Brentano geometry and it was equipped with a curved graphite monochromator. Data were taken with a 0.5 ° divergence slit, a receiving slit of 0.01 ° and a set of Soller slits with axial divergence of 1°. Data were recorded between 15 and 75 ° with a step size of 0.02 ° and a counting time of 0.5 s per step.

Density of sintered samples was determined by Archimedes method employing a lacquer as sealant agent. The average result was given after 5 measurements. On the other hand, the densities of the commercial $LiFePO_4$/C powder and was determined by using a helium pycnometer.

The microstructure of the samples was observed by using a field-emission scanning electron microscope (Zeiss, Merlin-type) using a secondary electron detector and an acceleration voltage of 5 kV. An EDX detector was employed for the compositional analysis of the samples. The presence of carbon coating of particles was evidenced by Transmission Electron Microscopy (TEM) by using a JEOL JEM 3000F microscope operating at 300 kV.

2.3 Electrochemistry

The electrochemical properties of the cathodes were studied in two-electrode coin cells

(type CR 2032). The cells were assembled in a dry Ar-filled glove box (< 1 ppm H_2O and O_2) with a foil of lithium as negative and reference electrodes. The electrolyte was a solution 1M of LiClO4 in (a) propylene carbonate (PC) or (b) propylene carbonate (PC), ethylene carbonate (EC) and dimethyl carbonate (DMC) in a volume ratio 1:1:1. In the case of the commercial powder composite, this cathode was prepared by mixing 80 wt. % of active material, 7.5 wt. % of acetylene black, 7.5 wt. % of graphite and 5 wt. % of Teflon as binder agent. The mixture was pressed onto a stainless-steel grid of 14 mm diameter under 8 tons cm^{-2} pressure and three glass microfiber filters (Whatman 1822-070) were used as separator. On the other hand, the extruded cathodes were self-supported and no binder neither metallic grid was employed. Also, no extra carbon was added to the extruded material and only two separators were used between the lithium foil and the extruded cathode. The dimensions of the extruded electrodes employed in coin cells were 0.5 mm thickness and (4.0 x 4.0) mm^2 surface area.

Electrochemical tests were carried out using a Biologic VMP3 multichannel tester. The galvanostatic tests were conducted using different current densities in the 4V-2V vs. Li^+/Li potential range at 20 °C, the 1C rate corresponding to 170 mA g^{-1}.

Impedance measurements were performed using a three-electrode cell in which the reference and the counter electrodes consisted, respectively, of a lithium wire in a separated compartment and a gold wire, both immersed along with the working electrode in a 1M $LiClO_4$ solution in PC/EC/DMC (1/1/1 vol.) as electrolyte. The frequency range was $8 \cdot 10^4$-$2 \cdot 10^{-3}$ Hz and the excitation signal 5.7 mV. The measurements were carried out when the equilibrium potential was reached, considering a variation less than 1 mV during 1 h.

3. RESULTS AND DISCUSSION

Powder Extrusion Moulding was selected for manufacturing thick LFP/C electrodes. In contrast to other processing techniques (i.e. powder compaction or tape casting), PEM allows obtaining binder-free and self-supported electrodes with high thickness and high areal capacity [15]. In the case of this work, the strategy was based on using an inert atmosphere during the

debinding and sintering steps in order to preserve the carbon coating of LFP particles and to prevent iron oxidation. Even after processing, the carbon content was slightly increased, coming from binder degradation.

3.1 Fabrication of self-supported LFP/C electrodes

3.1.1 Mixing and extrusion

The mixing torque, which corresponds to the effort required by the rotor blade mixer, is an indicator of the viscosity of the powder-binder mixture. So, the homogeneity of the mixture is estimated by the variation of the mixing torque over a period of time. Fig. 1a shows torque curves of feedstocks with different powder loadings. At the beginning of mixing process, small portions of binder components are added in the following order: polypropylene, paraffin wax and stearic acid and, subsequently, powder is incorporated into the mixture while an increment of torque is registered. Then, the torque reaches a constant value, called the steady-state value (τ), which indicates the mixture is homogeneous. The steady-state value is calculated as the average torque during the last 5 min of mixing. τ is reached in all the cases and increases with powder loading due to a higher viscosity of the mixture.

Fig. 1b represents the variation of the steady-state value with powder loading. In the graph, two different regions are identified at low and high powder loadings and a linear fit of the points of each region reveals an abrupt slope change. Firstly, from 50 to 52.5 vol. % of LFP/C, a pronounced increase of τ occurs as a consequence of the increased powder loading in the mixture, indicating a higher viscosity. However, for powder loadings above 52.5 vol. %, the steady-state torque remains almost constant. This behavior is totally unusual in powder-binder mixtures for PIM/PEM process and could be related with the fact of, first, there is not enough binder to cover the surface of powder particles and a fraction of them are in contact with each other. Secondly, all the LFP particles are coated by a very thin carbon layer, which acts as lubricant between particles allowing the powder loading to be increased without increasing the torque values. In addition, in the case of the feedstock with a 58 vol. % of powder loading, the visual aspect is slightly different from the rest of the feedstocks prepared, observing clearly

lack of binder covering the powder particles. In addition, for higher powder loadings, the torque value was not reached, indicating a bad distribution of the powder within the binder.

A rheological study of a feedstock is crucial to determine its ability to be extruded. Fig. 1c shows the variation of the viscosity with the shear rate for four feedstock formulations. As expected, the viscosity increases with the powder loading, achieving the maximum viscosity for the feedstock with 58 vol. %. All the samples display a pseudoplastic behavior which is the most convenient for extrusion process due to shear rate increases when feedstock is forced to pass through the nozzle and a decrease of viscosity is better to take place. Furthermore, most of the values are lower than 1000 Pa s between 100 and 10000 s^{-1}. These values are considered as a reference for a successful PIM process and in our specific case of powder extrusion moulding the maximum shear rate estimated in the twin-screw extruder is around 1000 s^{-1} [21]. The rheological behavior in a capillary test is quite well described by the Ostwald and De Waele power law [22,23]:

$$\eta = K \dot{\gamma}^{(n-1)}$$

where η is the viscosity, K is a constant, $\dot{\gamma}$ is the shear rate and n is the power law index. When n is lower than 1, the mixture presents a pseudoplastic behaviour, and the viscosity decreases when the shear rate increases.

The value of n indicates the degree of sensitivity of viscosity with the shear rate. The lower the value of n, the more sensitive is the viscosity to the shear rate and the more pseudoplastic is the feedstock. Comparing with LTO-feedstocks prepared with a similar binder formulation, [15] the n values are lower, being consequently even more sensitive to shear rate. Moreover, similar values were obtained for YSZ [11] and Ni-YSZ [12] feedstocks, which were in the range 0.31-0.41 and 0.17-0.30, respectively. In addition, in the case of Ni-YSZ, the flow index also decreased with the powder loading.

The variation of viscosity with the temperature is also important in extrusion process because fluctuation of temperature during extrusion takes place, producing stress concentration in the extruded part, resulting in cracking, distortion and other kind of defects. In general, the influence of temperature on viscosity can be expressed by the Arrhenius type equation:

$$\eta = \eta_0 \, e^{E_a/RT}$$

where E_a is the flow activation energy, η_0 is the viscosity at a reference temperature T and R is the ideal gas constant. Thus, the higher the temperature, the lower the viscosity. All the feedstocks follow this behavior, as observed in Fig. 1d for the feedstock with a powder loading of 55 vol. %. E_a was calculated from the slope of plots of the logarithmic viscosity against reciprocal of temperature considering the viscosity values at a shear rate of 1000 s^{-1} (Fig. 1e).

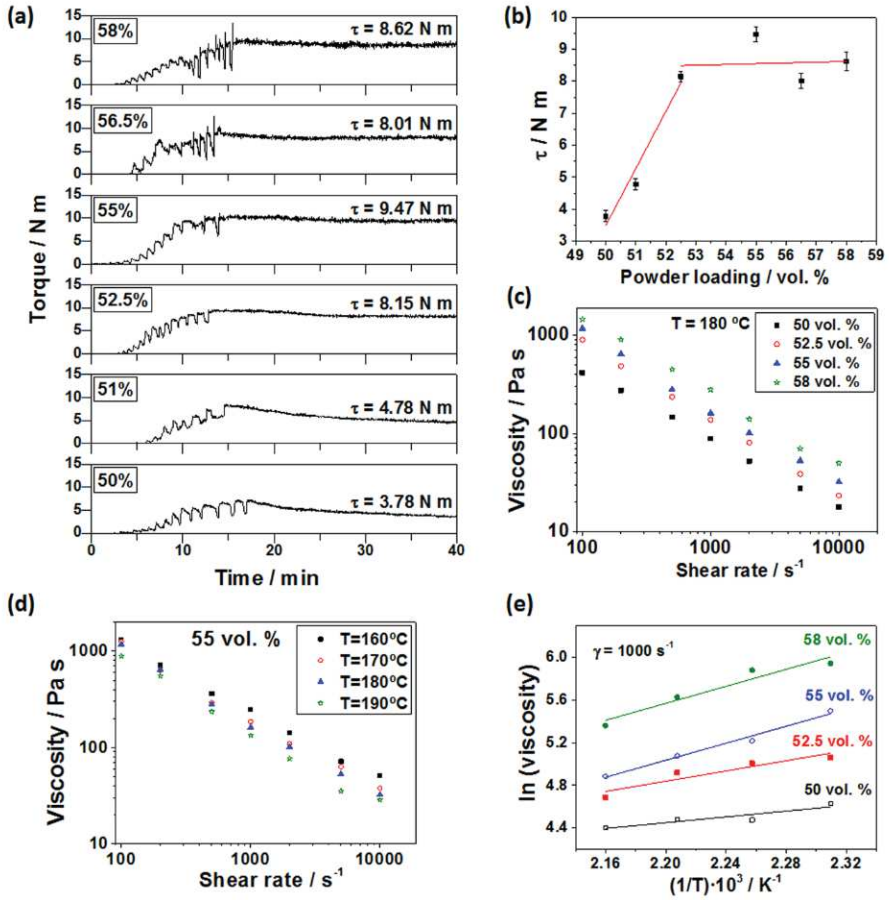

Fig. 1. (a) Torque against mixing time of feedstocks with different powder loadings. (b) Steady-state torque (τ) as a function of the powder loading. (c) Viscosity curves of LFP/C feedstocks with different powder loadings at 180 °C (453 K). (d) Viscosity curves for 55 vol. % feedstock at different temperatures. (e) Variation of viscosity with temperature for the different feedstocks. The data are adjusted following a linear fit according to an Arrhenius-type equation.

In Table 1, n values are collected. The flow index was determined from the slope of logarithmic plots of viscosity versus shear rate for feedstocks with different powder loadings.

The value of n decreases with both the powder loading and the temperature. This means that the feedstock is more able to reorganize with high powder loadings during the moulding process and it is more sensitive to the shear rate at high processing temperatures. The feedstock with the highest activation energy would be the most suitable for PEM, because when the feedstock comes out of the nozzle the decrease of the temperature will provoke an increase in the viscosity and hence a good geometry retention. Therefore, in our case those feedstocks with the highest powder loading (55 and 58 vol. %) are the most suitable for the PEM process. Moreover, the activation energy values of feedstocks with higher powder loadings are similar to those obtained for other feedstocks which have been previously successfully extruded such as Ni-YSZ [12]. In our case, the choice of the highest possible powder loading would be the most convenient condition [24], always providing that the viscosity achieve values lower than 1000 Pa s at a shear rate equal or higher than 100 s^{-1} [25]. Considering all the conclusions obtained from the mixture characterization, the feedstock with a powder loading of 55 vol. % is finally selected as the optimum one due to its suitable viscosity behavior. This feedstock prepared in a twin-screw extruder was analyzed by SEM in order to check the appropriate distribution of the powder throughout the binder.

Table 1

Power law index (n) and activation energy (E_a) of LFP/C feedstocks with different powder loadings. The linear regression coefficients associated to the fitting are given between brackets.

Powder loading (vol. %)	**n**				**E_a (kJ mol^{-1})**
	160 °C	170 °C	180 °C	190 °C	
50	0.35 (0.997)	0.34 (0.9997)	0.30 (0.9990)	0.30 (0.9994)	11.2
52.5	0.33 (0.994)	0.31 (0.991)	0.29 (0.98)	0.28 (0.9999)	20.0
55	0.29 (0.996)	0.25 (0.993)	0.22 (0.996)	0.22 (0.991)	33.1
58	0.29 (0.993)	0.26 (0.993)	0.24 (0.996)	0.22 (0.992)	33.1

Fig. 2a shows a SEM image of the feedstock in which powder LFP/C particles are embedded in the polymer matrix. Moreover, the geometry retention after extrusion is excellent (Fig. 2b). This

is related to the strong pseudoplastic behavior of the feedstock, which allows increasing easily the viscosity of the feedstock when it comes out from the extrusion nozzle.

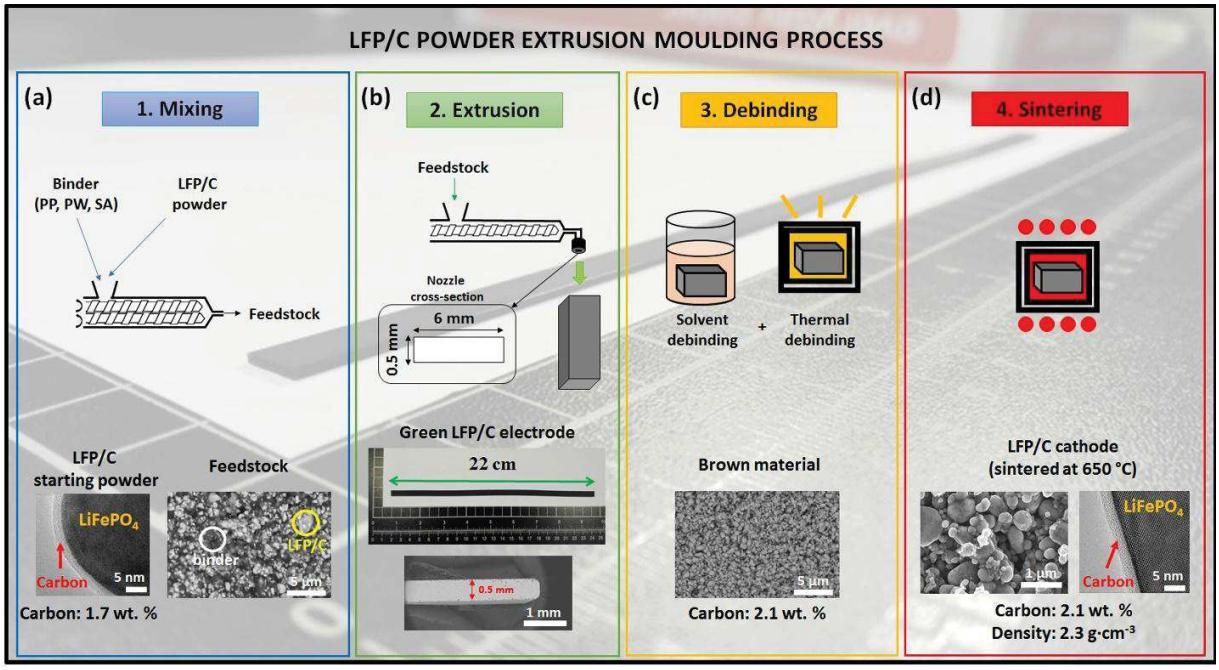

Fig. 2. Schematic representation of the different steps followed during the manufacturing of LFP/C electrodes by Powder Extrusion Moulding using a feedstock with a powder loading of 55 vol. % and a sintering temperature of 650 °C. Inside bottom figures details: (a) HREM image of starting LFP/C powder (left) and SEM image (back-scattered electrons) of the feedstock (right). (b) Photograph of a long green LFP/C electrode (top) and cross-section SEM image of the material (bottom). (c) SEM image of a brown LFP/C electrode. (d) For the sintered LFP/C cathode, SEM (left) and HREM (right) images.

3.1.2 Debinding

The debinding stage is performed in two different steps. Firstly, a solvent debinding is carried out for dissolving the lower molecular weight binder constituents (paraffin wax and stearic acid) in n-heptane at 50 °C. In this manner, the removal of these components creates a network of internal channels in the compact material favoring the evacuation of gases during the thermal step. In a second step, polypropylene is eliminated by thermal degradation. The thermal cycle consisted in two isothermal plateaus at 200 °C, to favor the elimination of undissolved paraffin wax and stearic acid, and at 450 °C, to carry out the thermal degradation of polypropylene. As mentioned before, all thermal treatments were performed under N_2

atmosphere to prevent Fe^{2+} oxidation and carbon combustion. Elemental analyses of 5 different samples after the debinding stage confirm that the carbon content is not only maintained ((2.10 ± 0.03) wt. %), but also increased compared to the starting LFP/C powder (1.70 ± 0.01 wt. %). This fact is explained by the incomplete elimination of the binder, which leaves some residual carbon in the material. The absence of organic components after the debinding step was confirmed by SEM (see Fig. 2c).

3.1.3 Sintering

XRD experiments were performed both on the starting LFP/C powder and on the extruded electrodes sintered at different temperatures. XRD patterns of extruded samples sintered at 650 and 850 °C are collected in Fig. 3a and compared with the diffraction pattern of the starting LFP/C powder. For sintering temperatures between 550 and 750 °C, the diffraction peaks of the patterns are assigned to $LiFePO_4$ (JCPDS 40-1499) and no evidence of any secondary phase was detected. However, from 850 °C to higher temperatures, the main diffraction peak of a secondary phase was observed and identified as Fe_2P (JCPDS 89-3680). This phase is formed, in presence of carbon, at high sintering temperatures.[26],[27] Although Fe_2P presents high electronic conductivity, it is inert for Li extraction-insertion.[28] For this reason, Fe_2P formation was avoided and samples sintered above 850 °C were not submitted to further studies. The presence of this phase is also confirmed by SEM (Fig. 3b), where small particles with bright contrast are clearly distinguished in BSE micrograph. EDS analysis of these bright particles indicates that Fe/P atomic ratio is 1.95, which is compatible with Fe_2P phase as revealed also by XRD. On the other hand, darker contrast particles whose Fe/P atomic ratio 1.03 corresponding to LFP, were observed. The microstructure of the extruded samples sintered between 550 and 750 °C basically does not change, and negligible variation was observed in the particle size of the extruded materials compared to the starting LFP/C powder, indicating the lack of sintering (see supplementary information- Fig. S2).

In all the cases, the materials present high porosity, which is beneficial to favor the electrochemical reactions as well as an adequate liquid electrolyte penetration. A SEM image of an extruded LFP/C electrode sintered at 650 °C is shown in Fig. 2d as an example of the

high porous microstructure of the ceramic electrodes. The density of the sintered materials was found to be the same for all sintering temperatures (65 % of theoretical value) and the total porosity was 35 %. This is confirmed by measuring the dimensional variation of the green samples after sintering, which was found to be independent on the sintering temperature.

HREM images of starting LFP/C powder (Fig. 2a) and extruded LFP/C sintered at 650 °C (Fig. 2d) show that particles of both powders present a homogeneous amorphous carbon coating of about 3 nm thickness. Moreover, elemental carbon analysis of both powders demonstrates again the retention of all the carbon after the sintering ((2.12 ± 0.03) wt. %). Thus, the extrusion process does not modify the carbon coating layer and the N_2 atmosphere was effective to protect it.

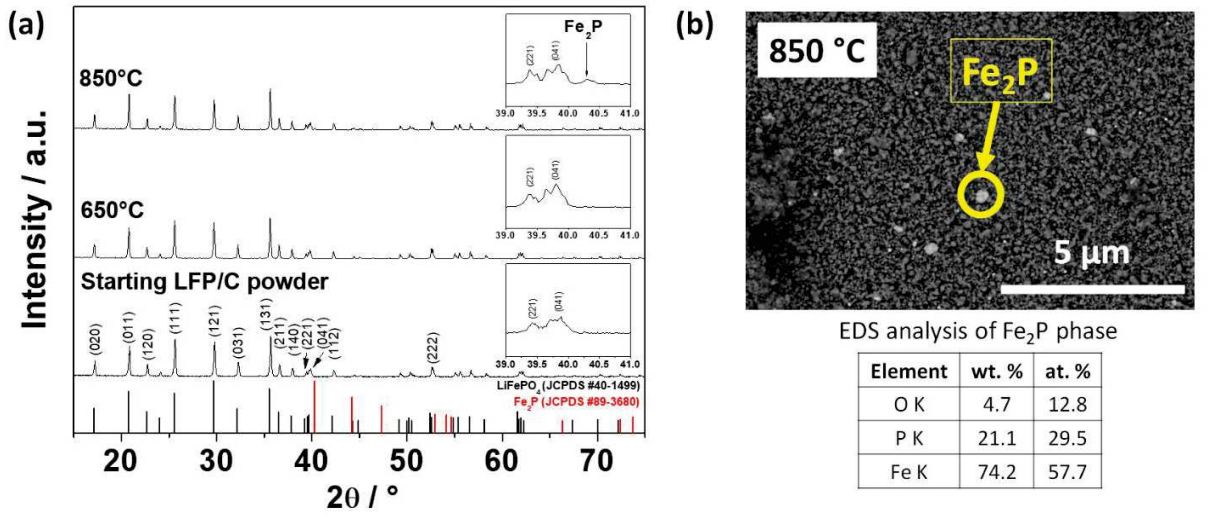

EDS analysis of Fe_2P phase

Element	wt. %	at. %
O K	4.7	12.8
P K	21.1	29.5
Fe K	74.2	57.7

Fig. 3. (a) XRD diffraction patterns of starting LFP/C powder and extruded LFP/C cathodes sintered under pure N_2 at 650 and 850 °C. Fe_2P secondary phase is marked in the figure inset with an arrow (↓). The peak data of the JCPDS cards of $LiFePO_4$ (#40-1499) and Fe_2P (#89-3680) are included as reference. (b) SEM image of extruded LFP/C electrode sintered at 850 °C and EDS data for Fe_2P phase.

3.2 Electrochemical performance of extruded LFP/C cathodes

3.2.1 Electrochemical performance dependence on processing and on samples thickness

In order to check the influence of PEM on the LFP/C powder, an extruded sample sintered at 600 °C was grinded in an agate mortar and its electrochemical performances were tested and compared with those of the fresh commercial LFP/C powder, which is used as the reference

electrode. In both cases the LFP/C electrodes were prepared as a conventional composite electrode by casting method from a mixture of active powder and additives. The ratio between these additives and active powder was exactly the same in both electrodes: 80 wt. % of active material, 7.5 wt. % of acetylene black, 7.5 wt. % of graphite and 5 wt. % of Teflon. Fig. 4a shows the corresponding charge/discharge curves for the first cycle at a low C rate (C/20). Both samples exhibit a flat voltage plateau at 3.48 and 3.39 V for the charge and discharge, respectively. Moreover, a similar low hysteresis is observed. Both materials have a reversible capacity of 162 mA h g^{-1}, corresponding to a lithium uptake of 0.95 Li per $LiFePO_4$, and display similar cycling behavior (included in supplementary information- Fig. S3) confirming again that the manufacturing process, here proposed, does not modify the original characteristic of the starting powder.

Fig. 4b depicts the typical charge and discharge curves, achieved respectively at C/20 and C/100, for an additive-free LFP/C electrode extruded at 600 °C. The shape of the curve is basically the same than that of the conventional composite electrodes prepared with fresh commercial powder (Fig. 4a). A reversible specific capacity of about 170 mA h g^{-1}, close to the theoretical one, is obtained that proves that the totality of the active material present in this 0.5 mm thick electrode participates in electron transfer. While the lithiation process carried out at C/100 takes place at a potential value close to the composite electrodes ones, the charge process at C/20 indicates the existence of a slight polarization phenomenon (3.55 V instead of 3.48 V vs. Li^+/Li) probably due to a much lower carbon content compared to the composite electrode.

This hypothesis is confirmed by the evolution of the cycling curves as the C rate increases (Fig. 4c). The hysteresis between charge and discharge rises from 340 mV to 900 mV while C rate increases from C/10 to C/2. This polarization entails the system reaches the upper cut-off voltage before the end of the charge process. Hence, the higher the C rate the lower the efficiency of the charge that drastically impacts the recovered available capacities (118, 94 and 10 mA h g^{-1} for respectively C/10, C/5 and C/2). Besides, at C rates exceeding C/2, the polarization of the electrode is so high that no capacity is achieved.

This trend can be strongly limited with the use of a thinner extruded sample 0.3 mm thick

600 °C (Fig. 4d), obtained by grinding the 0.5 mm thick electrode. Indeed, at C/10, the capacity increases from 118 to 138 mA h g^{-1} and the polarization decreases from 340 to 280 mV. At higher C rates, while the hysteresis remains about the same, capacity values are also significantly improved with 112 mA h g^{-1} at C/5 and 41 mA h g^{-1} at C/2.

3.2.2 Dependence of extruded electrodes performances on electrolyte viscosity

Besides unoptimized interparticle electronic contacts in these extruded electrodes, another limitation might arise from their unoptimized impregnation with the electrolyte, especially as their thickness increases.

In order to assess the dependence on extruded electrode performances on their wetting by the electrolyte, we compared 2 electrolytes. The cycling curves presented so far were recorded using a molar solution of $LiClO_4$ in propylene carbonate (PC). This solvent has, at 25 °C, a viscosity higher than the usual electrolytes based on mixtures of carbonates [29]. For these reasons, we tested the electrochemical performances of our extruded electrodes in a molar solution of $LiClO_4$ in a mixture of propylene carbonate (PC), ethylene carbonate (EC) and dimethyl carbonate (DMC) (1/1/1 in volume). Fig. 4e clearly depicts the advantages of using this electrolyte. Higher capacities than with the PC electrolyte (cf. Fig. 4c) are reached with the ternary liquid electrolyte with an improvement of 30-50 %.

For the lowest C rates, values comparable to those obtained with the commercial powder composite LFP/C electrode (Fig. 4f) are obtained (156 and 137 mA h g^{-1} compared to 158 and 146 mA h g^{-1} respectively at C/10 and C/5). However, as soon as the current densities exceed C/2, this ternary liquid electrolyte does not enable the decrease in polarization and available capacities, although improved, always remain much lower than those obtained in the case of conventional LFP composite electrodes. As a conclusion, a decrease in the viscosity of electrolyte led to improved performances that we ascribe to a better penetration of the electrolyte and to a decreased polarization, improving the rate capability of the 0.5 mm thick extruded material. In this way, all the experiments that follow were carried out using 1 M $LiClO_4$ in PC/EC/DMC. Besides, same specific capacities for reference and extruded

electrodes correspond to areal capacities of 3.8 mA h cm^{-2} and 13.7 mA h cm^{-2}, respectively. Thus, the areal capacity for the thick extruded electrode is found to be 3.5 fold higher than the composite one.

3.2.3 Dependence of extruded electrodes performances on the sintering temperature

The effect of the sintering temperature of extruded electrodes on electrochemical performances has also been studied. Cycling curves registered at C/5 for different sintering temperatures are gathered in Fig. 5a. The lowest sintering temperature, 550 °C, harms a little the capacity with 120 mA h g^{-1} at C/5 against 130 mA h g^{-1} for sintering temperatures between 600 and 650 °C. Also, higher polarization is observed (about 850 mV against 600 mV for 600 and 650 °C). When the sintering temperature is fixed at 750 °C, polarization is quite the same as those observed for 600 or 650 °C while the capacity is lower, comparable to the capacity obtained for 550 °C. At last, the electrode sintered at the highest temperature of 850 °C is unable to deliver any capacity. These results can be correlated to the electrodes grain growth. Indeed, SEM images (Fig. S2) highlighted that in the case of 850 °C, the biggest particle size was obtained. This large grain size could make the carbon coating thinner or heterogeneous, so that the continuous pathway for electronic conduction could be interrupted, worsening the electrochemical response of the electrode. Moreover, XRD and EDS experiments indicated the presence of Fe_2P in the electrode sintered at 850 °C (cf. Fig. 3a) that is known to be inactive for Li extraction-insertion. The larger LFP grain size also has a detrimental effect on the kinetics of lithium transport since the length of diffusion pathway increases.

On the other hand, at C/5, between all the extruded electrodes, the one sintered at 650 °C presented the highest capacity values. However, at C/2 the extruded materials presented very low capacity (Fig. 5b) associated to high polarization. Hence the sample sintered at 650 °C was selected as the one with the best electrochemical response at low C rates (C/10 and C/5) and was studied deeply, as follows.

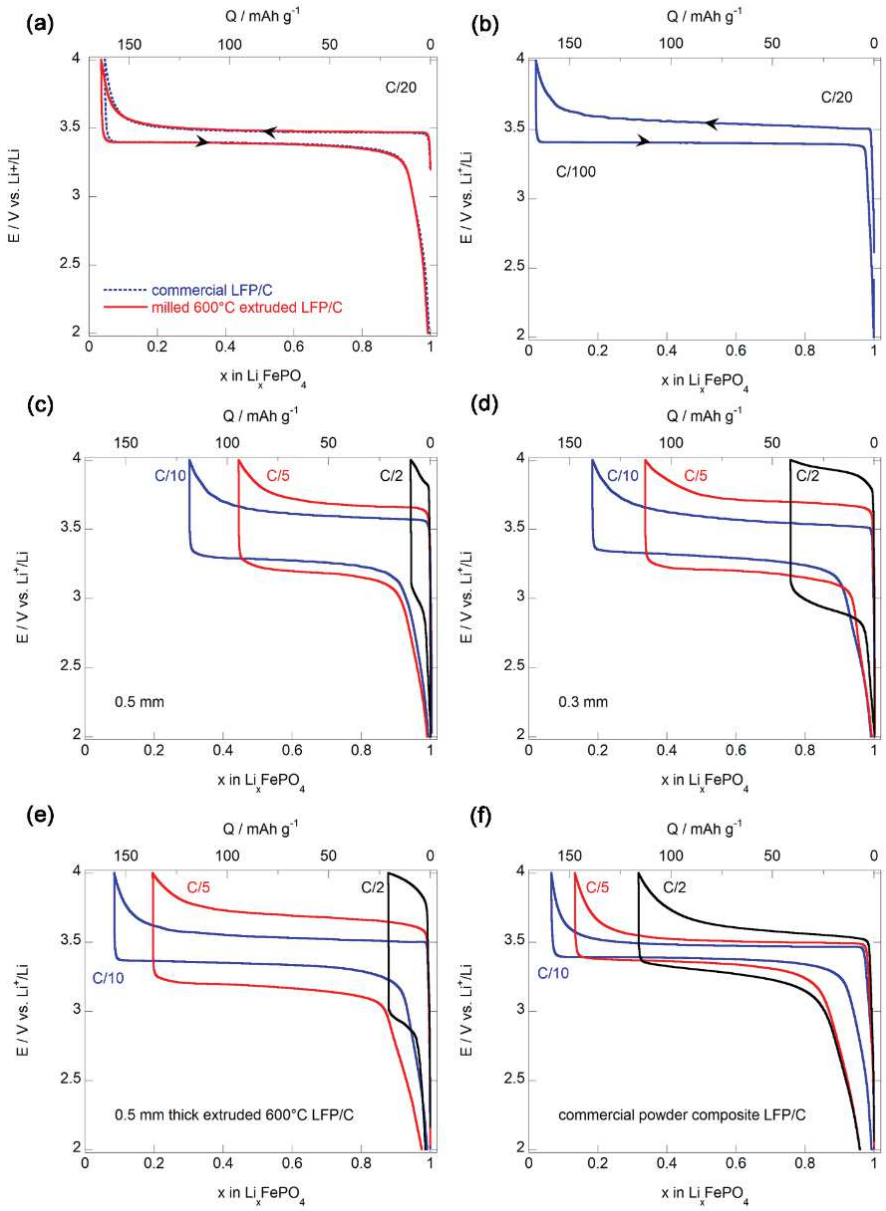

Fig. 4. (a) Charge/discharge first cycles registered at C/20 in PC/$LiClO_4$ 1 mol L^{-1} for a commercial LFP/C powder electrode (dashed blue curve) and for a grinded-600°C extruded LFP/C powder electrode (full red curve). (b) First charge (C/20) and discharge (C/100) curves registered in PC/$LiClO_4$ 1 mol L^{-1} for a 600°C extruded LFP/C 0.5 mm thick electrode. Charge/discharge curves registered in PC/$LiClO_4$ 1 mol L^{-1} at C/10 (black), C/5 (red) and C/2 (blue) with a (c) 0.5 mm thick and a (d) 0.3 mm thick 600°C extruded LFP/C electrodes. Charge/discharge curves registered in PC/EC/DMC $LiClO_4$ 1 mol L^{-1} for (e) a 0.5 mm thick extruded 600 °C LFP/C electrode and for (f) a commercial powder composite LFP/C electrode at C/10 (black), C/5 (red) and C/2 (blue).

As the self-supported LFP/C electrodes present at C/10 capacities comparable to those obtained with commercial powder electrodes, it appears interesting to verify whether this kind of additive-free electrodes could cycle over a large number of charge/discharge sequences without physical damage. For this purpose, the evolution of the capacities available during the first twenty charge/discharge cycles, at C/10, is reported in Fig. 5c for an extruded 650 °C LFP/C electrode. For comparison, values obtained in the same conditions for the commercial powder composite LFP/C electrode are overlaid. Clearly, at this moderate C rate, both technologies allow to reach the same performances, indicating the good mechanical stability of the extruded electrode over at least 20 cycles. It is noticeable that areal and volumetric capacity are greatly enhanced in the extruded electrode respect to the composite one used as reference (about 4 times and 1.5 higher, respectively) (see supplementary information-Fig. S4).

This new technology of extruded electrodes deserves all our attention as they are easy to handle and no additives are used. Consequently, the available capacities, brought back to the total electrode mass and not to the mass of active material in the electrode, are significantly greater, at least by 20 %, than those achieved with the usual composite LFP electrode (Fig. 5d).

3.2.4 Cut-off voltage

As already mentioned, the intrinsic polarization observed in the extruded electrodes, impedes the charge process at 4 V, especially at C/2. Hence, a higher oxidation voltage as new upper limit could allow to complete the charge process at C/2 and, then to enhance the recovered capacity. To avoid electrolyte decomposition, a maximum voltage of 4.5 V is used for C rates between C/10 and C/2.

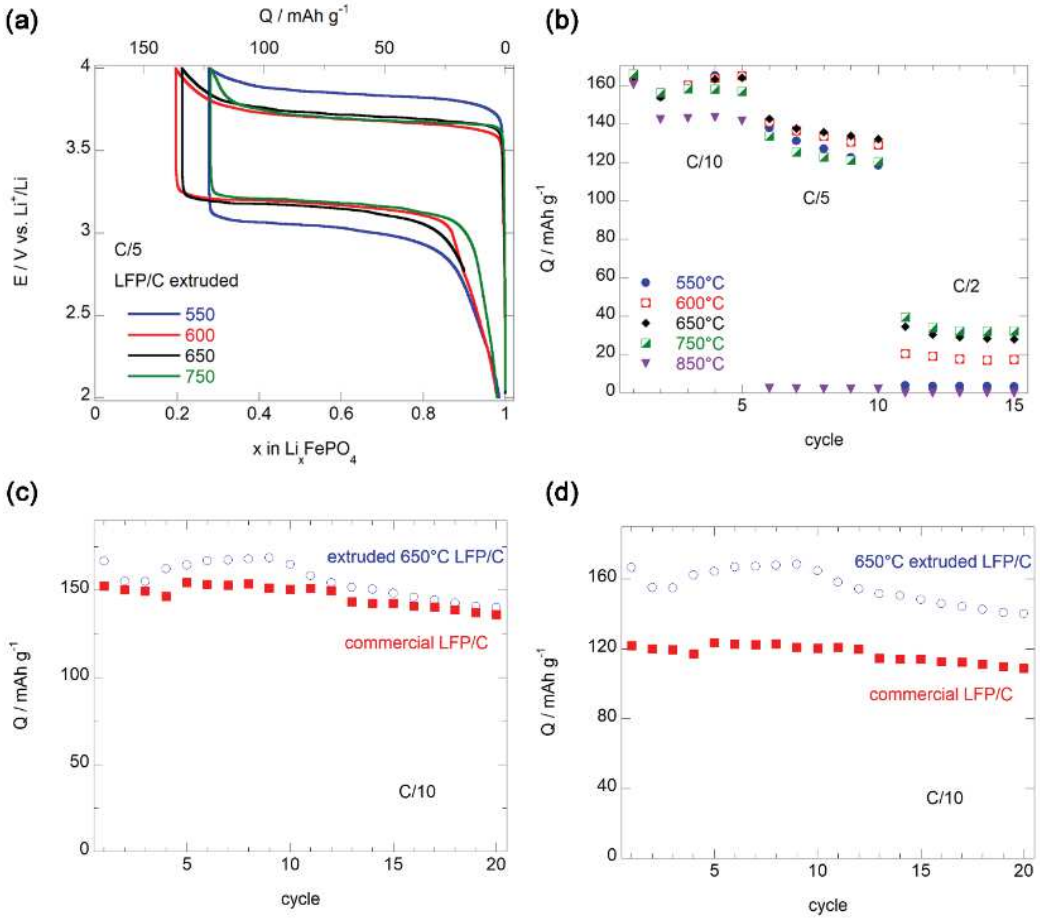

Fig. 5. Influence of sintering temperature for 0.5 mm thick extruded LFP/C electrodes in PC/EC/DMC $LiClO_4$ 1 mol L^{-1} on (a) the shape of cycling curves registered at C/5 and on (b) rate capability. (c) Evolution of specific capacity as a function of cycle number at C/10 in PC/EC/DMC $LiClO_4$ 1 mol L^{-1} for a 0.5 mm thick extruded 650 °C LFP/C electrode (empty markers) and for a commercial powder composite LFP/C electrode (full markers). (d) Evolution of the capacity, expressed in mA h per gram of electrode (mass capacity), as a function of cycle number at C/10 in PC/EC/DMC $LiClO_4$ 1 mol L^{-1} for a 0.5 mm thick extruded 650 °C LFP/C electrode (empty markers) and for a commercial powder composite LFP/C electrode (full markers).

The rate capability of extruded 650 °C electrodes in the enlarged 4.5 V-2 V potential window is reported in Fig. 6a with some of the corresponding typical cycling curves selected for C/10, C/5 and C/2. The results are compared with those achieved in the previous 4V-2V range reported Fig. 6b. For moderate C rates (C/10), no significant change in the capacity

value around 165 mA h g^{-1} is observed. However, for C/5 the capacity already increases from 138 to 156 mA h g^{-1}. At C/2 more than twice the capacity is obtained in the extended potential range with 82 mA h g^{-1} against about 35 mA h g^{-1}.

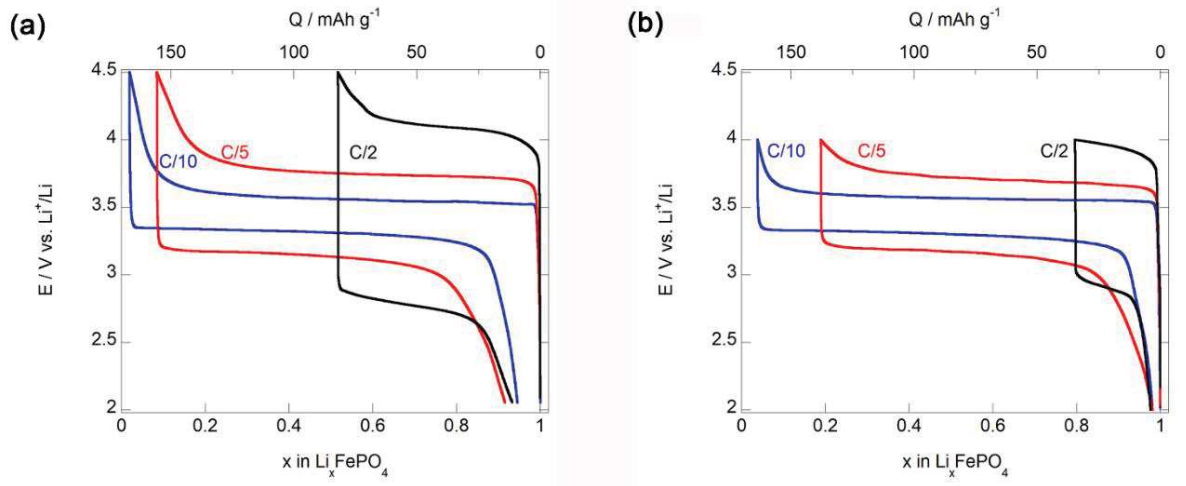

Fig. 6. Charge/discharge curves registered in PC/EC/DMC $LiClO_4$ 1 mol L^{-1} with a 0.5 mm thick extruded 650°C LFP/C at C/10 (blue), C/5 (red) and C/2 (black) (a) between 2.0 V and 4.5 V and (b) between 2.0 V and 4.0 V.

3.2.5 Electrochemical Impedance Spectroscopy

A study by electrochemical impedance spectroscopy was carried out in a three-electrodes cell, on a 0.5 mm thickness extruded 650 °C electrode, for different lithium contents in Li_xFePO_4 (with x = 0, 0.2, 0.5, 0.9 and 1). The measurements have been carried out during the second charge-discharge cycle. The corresponding Nyquist diagrams are gathered in Fig. 7a. Such diagrams are typical of insertion compounds [30]. They all exhibit different contributions characterized by (see inset): (1) the electrolyte resistance R_{elec}, given by the intercept of the abscissa and the starting point of a semicircle at high frequencies; (2) a well-defined semicircle at high frequencies corresponding to the charge transfer resistance R_{CT}; (3) a Warburg region for diffusion process at medium frequencies, characterized by a 45 ° line with respect to the real axis; (4) a quasi-vertical line ascribed to the finite diffusion at low frequencies. All these characteristic values have been determined and compared to those obtained in the case of the reference electrode, which contains exactly the same amount of active material (13.7 mg in

both electrodes). At first, it can be noticed that the electrolyte resistance is comparable for both electrodes, highlighting no additional interfacial resistance in the case of PEM. This point is interesting because discards a possible poor contact between our extruded electrode and the current collector due to its rigidity, hypothesis that could have explained the huge polarization observed and already discussed as soon as the C rate increases. About the charge transfer resistance, a quite stable value of 250 Ω is obtained for $0 \leq x < 1$. It is a little bit higher for x = 1 with 282 Ω, but all these values are higher, by one order of magnitude, than for the reference LFP/C electrode (see supplementary information-Table S1). This indicates slower kinetics for the electron transfer in the extruded electrode than in the conventional composite ones, and such a discrepancy could be related with the lower carbon content in the extruded sample (2.1 wt. % against 16.7 wt. % in the reference LFP/C electrode). This fact is in agreement with the evolution of the cathode impedance |Z| of the extruded electrode (Fig. 7b) much higher by a factor 4, than the commercial one, whatever the x value in composite. This well illustrates the difference in the electrode technology used in both cases.

Besides, the characteristic frequency at the top of the semicircle (f_{max} according to the scheme Fig. 7a inset) is in both cases independent of the lithium content in the material. About 100 Hz for the commercial LFP/C electrode while its value is close to 10 Hz for the extruded one. It is possible to deduce the double layer capacitance C_{DL} from this frequency and the charge transfer resistance, using the relation [30]:

$$C_{DL} = \frac{1}{2\pi R_{CT} f_{max}}$$

Very close values are found, 48 µF and 50 µF for the commercial LFP/C electrode and for the extruded LFP/C electrode, respectively. This indicates that the electroactive surface areas are equivalent for the same involved active material mass (13.7 mg) while geometrical areas are very different (ratio commercial/extruded ≈ 3). This finding justifies that capacities close to the theoretical one are achieved with this kind of additive-free electrode where all the LFP grains take part to the electrochemical Li extraction-insertion. The proposed here additive-free LFP electrode obtained by PEM technology homogeneously and quantitatively works. The Warburg domain can be exploited over the composition range $0.2 \leq x \leq 0.9$, using the equation [30]:

$$D_{Li} = \left(\frac{V_M}{\sqrt{2}nFS}\frac{dE}{dx}\frac{1}{A_S}\right)^2$$

where V_M is the molar volume of the compound (44.8 cm^3 mol^{-1}); n the number of electron; S is the geometric surface area of the electrode (S = 0.4 cm^2); $\frac{dE}{dx}$ is the slope, at fixed x, of the curve E = f(x) (Fig. 4b) that corresponds to the equilibrium potential composition curve and As the slope of the line obtained by representing Re(Z) as a function of $\frac{1}{\sqrt{\omega}}$ corresponding to the Warburg region.

For the extruded electrode, lithium diffusion coefficient around $5 \cdot 10^{-12}$ cm^2 s^{-1} is found in the $0.2 \leq x \leq 0.9$ composition range. The $\frac{dE}{dx}$ slope value is 8.9·10-2 V in this range of composition corresponding to the biphasic domain where $LiFePO_4$ and $FePO_4$ coexist. It is also possible to use the limiting frequency f_L^*, defined by the intercept between the Warburg line and the quasi vertical line, as illustrated in the inset Fig. 7a. According to the equation [30]:

$$f_L^* = \frac{D_{Li}}{L^2}$$

in which L is the maximum length of the diffusion pathway corresponding to half the grain size (100 nm). Very close D_{Li} values are obtained ($8 \cdot 10^{-12}$ cm^2 s^{-1} for x = 0.2 and x = 1). Higher D_{Li} values by one order of magnitude are found in the case of commercial LFP/C powder. We think this apparent difference in the lithium diffusion kinetics is not to be related to an intrinsic property of the LFP material but rather reflects the electrode technology used in each case. The lower electronic percolation in the case of the extruded electrodes is responsible of the lower kinetics that limit the use of this concept at current densities lower than C/5.

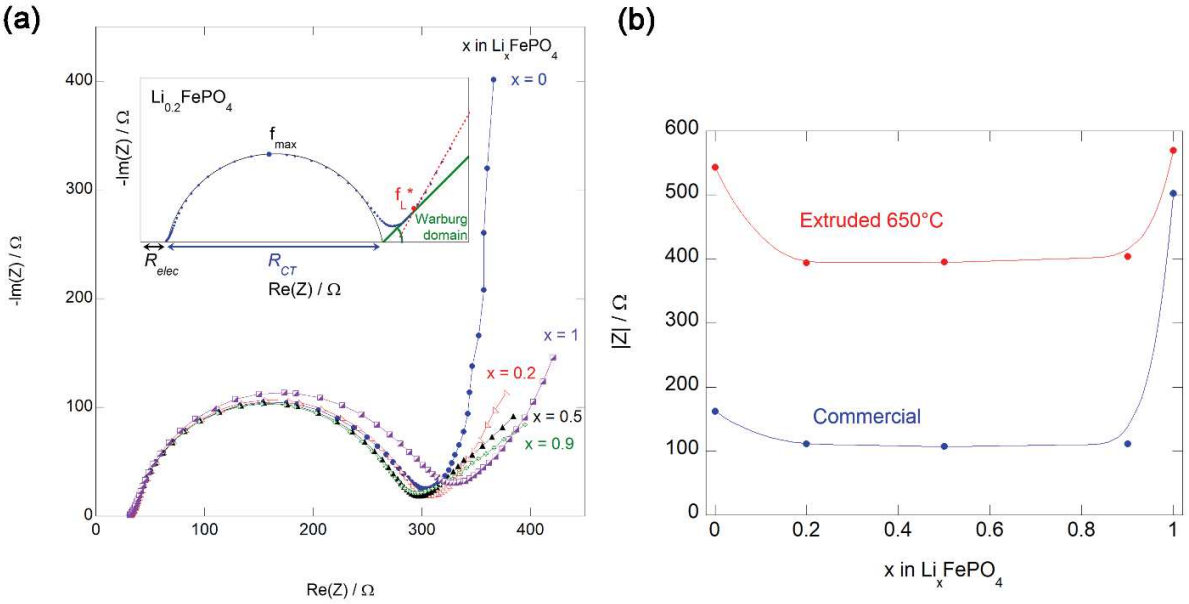

Fig. 7. (a) Nyquist diagrams of a 650 °C extruded electrode (S = 0.4 cm^2) for different charge states. (b) Comparison of total impedance |Z| between conventional LFP/C electrode and 650 °C extruded electrode for different charge states.

3.3 Discussion

The main challenges of future lithium batteries are higher safety, higher power and energy, wider operating temperature range and lower cost per kW h. The ASSBs seem excellent candidates to achieve these ambitious objectives. However, they still face many challenges before the technology is ready for the market. A plausible approach is the use of additive-free ceramic electrodes.

However, when the activity on these electrodes was initiated, [31] not so long ago, the main concerns were the kinetics or mass transfer issues besides to the eventual collapse of the ceramic electrode associated with volume changes during the charge-discharge cycles, being unimaginable to reversibly cycle so thick electrodes. Thus, regarding ASSB State Of Art, the

electrodes are shaped into thin films of a few micrometers. In an attempt to improve the electrode thickness of ASSB, Aboulaich *et al.* [32], sandwiched a glass-ceramic electrolyte (LAG: $Li_{1.5}Al0.5Ge1.5(PO_4)_3$) by composite electrodes made of LAG, Carbon Super P, and active materials i.e. $Li_3V_2(PO_4)_3$ for the negative and LFP for the positive. Owing to the low content in active materials of their composite electrodes they conclude: "the first impact of our all-solid-state batteries is expected in niche applications where high temperature operation (> 120°C) is necessary". 470 µm-thick LTO electrodes made by PEM were found to cycle with a high coulombic efficiency over up to 50 charge/discharge cycles. Nonetheless the best cycling performances were obtained at low C-rates, C/20 and C/24.[15],[31] At C/12 rate, LTO still retains high volumetric and areal capacities but with a significant drop (13 %) compared to those obtained at C/24. It must be highlighted that, with roughly the same thickness, the extruded LFP/C demonstrates improved cycling performances compared to LTO, especially at C/10 rate. Whatever the ceramic (electrolyte or not), it suffers from a low shock resistance that imposes its shaping into thicknesses of several hundred micrometers. This is a handicap for ceramic electrolytes as it decreases their ionic conductance, however high thickness is, from now on (these data), an indisputable advantage for ceramic electrodes as it allows markedly increasing the areal capacity. Increasing areal capacity, thanks to extruded electrodes, results is an efficient cost-cutting tool as it allows decreasing the surface of costly components as (i) current collectors (copper) (ii) macroporous separators and (iii) electrolyte volume. Moreover, these thick ceramic electrodes improve the thermomechanical stability of related batteries. If their current cycling performances (high C rates) are still lower than those of conventional composite electrodes, batteries based on these new electrodes are well adapted to the storage of renewable electricity. Furthermore, this new generation of electrodes will facilitate the recycling of batteries, a critical aspect to consider in future commercial batteries. We believe that there are huge margins of progress given that industrial scale up is possible. Unlike other more attractive solutions proposed by Aboulaich *et al.* [32] and, more recent, by Seznec *et al.* [17] in which SPS (Spark Plasma Sintering) is involved, the technology here proposed, seems more feasible process for scale-up. Conversely PEM, a variant of the industrial process PIM, is a simple and easily scalable technology.

4. Conclusions

In this experimental work, Powder Extrusion Moulding (PEM) process is optimized for the preparation of thick LFP electrodes of ~500 μm thickness. All the relevant parameters (i) feedstock content in active material (ii) sample thickness (iii) sintering temperature and (iv) electrolyte viscosity were studied. Despite the very high thickness of the ceramic electrodes, they exhibit a very good electrochemical performance at relatively low C-rates (between C/10 and C/24), being very similar to those of the conventional composite electrodes used as reference. This unexpected result is reached thanks to the high porosity of the electrodes (35 %), which permits the penetration of the liquid electrolyte into the thick material. The sintering under inert N_2 atmosphere allows keeping the homogeneous carbon coating of 0.3 nm in the particles, which ensure the electrical percolation. As a result, high specific capacity and very high areal capacity (13.7 mA h cm^{-2}) were obtained. This value is approximately 4 times the areal capacity of the composite electrode used as reference. These results pave the way to a new generation of high performances and environmentally sustainable Li batteries, including LIBs, with a favourable electrode to current collector (and separator) ratio per stack volume and due to the simplicity of electrodes facilitate the recycling of the whole battery. While new materials can face processing issues, PEM is a mature technology prone to be used first at semi-pilot scale, then possibly at industrial scale. Moreover, PEM allows using starting powders of fairly low sophistication thus decreasing the overall cost of electrodes. Nonetheless several aspects of the process deserve to be thoroughly investigated as the formulation (aid-process binders, possible fillers) and the sintering temperature in order to improve the electrode performances *e.g.* in terms of electronic conductivity to perform charge/discharge cycles at C rates > C/10.

Author information

Corresponding Author

* E-mail: alvar@ing.uc3m.es

Author Contributions

The manuscript was written through contributions of all authors. All authors have given approval to the final version of the manuscript.

Declaration of competing interest

There are not conflicts to declare.

Acknowledgement

Authors would like to thank financial support received from Spanish Government MICINN (MAT2016-78362-C4-3-R project), and Madrid regional Government (MATERYENER3CM S2013/MIT-2753 program). They also thank the ICTS-Centro Nacional de Microscopía Electrónica (UCM, Madrid) for instrumental facilities and Dr. Esteban Urones for fruitful discussion about carbon coating. J.-Y. Sanchez acknowledges the CONEX Programme, funding received from Universidad Carlos III de Madrid, the European Union's Seventh Framework Programme for research, technological development and demonstration (Grant agreement n. 600371), Spanish Ministry of Economy and Competitiveness (COFUND2013-40258) and Banco Santander. C. de la Torre-Gamarra would like to thank Universidad Carlos III de Madrid for the mobility grant received for her predoctoral stay at Institut de Chimie et des Matériaux Paris Est (Thiais – France).

References

[1] K. Mizushima, P.C. Jones, P.J. Wiseman, J.B. Goodenough, $LixCoO_2$ ($0<x\leq1$): A new cathode material for batteries of high energy density, Solid State Ionics. 15 (1980) 783–789. https://doi.org/10.1016/0167-2738(81)90077-1.

[2] B. Dunn, B. Dunn, H. Kamath, J. Tarascon, Electrical energy storage for the gridfor the Grid : A Battery of choices, Sci. Mag. 334 (2011) 928–936. https://doi.org/10.1126/science.1212741.

[3] A. Mauger, C.M. Julien, Critical review on lithium-ion batteries: are they safe? Sustainable?, Ionics (Kiel). 23 (2017) 1933–1947. https://doi.org/10.1007/s11581-017-2177-8.

[4] L.X. Yuan, Z.H. Wang, W.X. Zhang, X.L. Hu, J.T. Chen, Y.H. Huang, J.B. Goodenough, Development and challenges of $LiFePO_4$ cathode material for lithium-ion batteries, Energy Environ. Sci. 4 (2011) 269–284. https://doi.org/10.1039/c0ee00029a.

[5] N. Nitta, F. Wu, J.T. Lee, G. Yushin, Li-ion battery materials: Present and future, Mater. Today. 18 (2015) 252–264. https://doi.org/10.1016/j.mattod.2014.10.040.

[6] J.S. Wang, P. Liu, E. Sherman, M. Verbrugge, H. Tataria, Formulation and characterization of ultra-thick electrodes for high energy lithium-ion batteries employing tailored metal foams, J. Power Sources. 196 (2011) 8714–8718. https://doi.org/10.1016/j.jpowsour.2011.06.071.

[7] L. Hu, F. La Mantia, H. Wu, X. Xie, J. McDonough, M. Pasta, Y. Cui, Lithium-ion textile batteries with large areal mass loading, Adv. Energy Mater. 1 (2011) 1012–1017. https://doi.org/10.1002/aenm.201100261.

[8] H. Zheng, J. Li, X. Song, G. Liu, V.S. Battaglia, A comprehensive understanding of electrode thickness effects on the electrochemical performances of Li-ion battery cathodes, Electrochim. Acta. 71 (2012) 258–265. https://doi.org/10.1016/j.electacta.2012.03.161.

[9] M. Singh, J. Kaiser, H. Hahn, Thick Electrodes for High Energy Lithium Ion Batteries, J. Electrochem. Soc. 162 (2015) A1196–A1201. https://doi.org/10.1149/2.0401507jes.

[10] J. Kasemchainan, P.G. Bruce, All-Solid-State Batteries and their Remaining Challenges, Johnson Matthey Technol. Rev. 62 (2018) 177–180. https://doi.org/10.1595/205651318X696747.

[11] T. Jardiel, M.E. Sotomayor, B. Levenfeld, A. Várez, Optimization of the processing of 8-YSZ powder by powder injection molding for SOFC electrolytes, Int. J. Appl. Ceram. Technol. 5 (2008) 574–581. https://doi.org/10.1111/j.1744-7402.2008.02286.x.

[12] B.I. Arias-Serrano, M.E. Sotomayor, A. Várez, B. Levenfeld, H. Monzón, M.A. Laguna-Bercero, A. Larrea, High-performance Ni-YSZ thin-walled microtubes for anode-supported solid oxide fuel cells obtained by powder extrusion moulding, RSC Adv. 6 (2016) 19007–19015. https://doi.org/10.1039/c5ra28183k.

[13] H. Monzón, M.A. Laguna-Bercero, A. Larrea, B.I. Arias, A. Várez, B. Levenfeld, Design of industrially scalable microtubular solid oxide fuel cells based on an extruded support,

in: Int. J. Hydrogen Energy, 2014: pp. 5470–5476.

https://doi.org/10.1016/j.ijhydene.2014.01.010.

[14] M.E. Sotomayor, L.M. Ospina, B. Levenfeld, A. Várez, Characterization of 430L porous supports obtained by powder extrusion moulding for their application in solid oxide fuel cells, Mater. Charact. 86 (2013) 108–115. https://doi.org/10.1016/j.matchar.2013.09.020.

[15] M.E. Sotomayor, C. de la Torre-Gamarra, W. Bucheli, J.M. Amarilla, A. Varez, B. Levenfeld, J.-Y. Sanchez, Additive-free $Li_4Ti_5O_{12}$ thick electrodes for Li-ion batteries with high electrochemical performance, J. Mater. Chem. A. 6 (2018) 5952–5961. https://doi.org/10.1039/C7TA10683A.

[16] X. Feng, M. Ouyang, X. Liu, L. Lu, Y. Xia, X. He, Thermal runaway mechanism of lithium ion battery for electric vehicles: A review, Energy Storage Mater. 10 (2018) 246–267. https://doi.org/10.1016/j.ensm.2017.05.013.

[17] R. Elango, A. Demortière, V. De Andrade, M. Morcrette, V. Seznec, Thick Binder-Free Electrodes for Li–Ion Battery Fabricated Using Templating Approach and Spark Plasma Sintering Reveals High Areal Capacity, Adv. Energy Mater. 8 (2018) 1–8. https://doi.org/10.1002/aenm.201703031.

[18] G. Delaizir, V. Viallet, A. Aboulaich, R. Bouchet, L. Tortet, V. Seznec, M. Morcrette, J.M. Tarascon, P. Rozier, M. Dollé, The stone age revisited: Building a monolithic inorganic lithium-ion battery, Adv. Funct. Mater. 22 (2012) 2140–2147. https://doi.org/10.1002/adfm.201102479.

[19] Y. Kato, S. Shiotani, K. Morita, K. Suzuki, M. Hirayama, R. Kanno, All-Solid-State Batteries with Thick Electrode Configurations, J. Phys. Chem. Lett. 9 (2018) 607–613. https://doi.org/10.1021/acs.jpclett.7b02880.

[20] M.E. Sotomayor, C. de la Torre-Gamarra, B. Levenfeld, J.-Y. Sanchez, A. Varez, G.-T. Kim, A. Varzi, S. Passerini, Ultra-thick battery electrodes for high gravimetric and volumetric energy density Li-ion batteries, J. Power Sources. 437 (2019) 226923. https://doi.org/10.1016/j.jpowsour.2019.226923.

[21] I. Manas-Zloczower, Mixing and compounding of polymers: Theory and Practice, 2nd edition, Hanser, Munich, 2009.

[22] A. de Waele, Viscometry and plastometry, J. Oil Colour Chem. Assoc. 6 (1923) 33–69.

[23] W. Ostwald, Speed function of viscosity of disperse systems I, Kolloid-Zeitschrift. 36 (1925) 99–117.

[24] Y. Li, L. Li, K.A. Khalil, Effect of powder loading on metal injection molding stainless steels, J. Mater. Process. Technol. 183 (2007) 432–439. https://doi.org/10.1016/j.jmatprotec.2006.10.039.

[25] B.C. Mutsuddy, Injection-Molding research paves way to ceramic engine parts, Ind. Res. Dev. 25 (1983) 76–80.

[26] S.-Y. Chung, J.T. Bloking, Y.-M. Chiang, Electronically conductive phospho-olivines as lithium storage electrodes, Nat. Mater. 1 (2002) 123–128. https://doi.org/10.1038/nmat732.

[27] Y. Xu, Y. Lu, L. Yan, Z. Yang, R. Yang, Synthesis and effect of forming Fe_2P phase on the physics and electrochemical properties of LiFePO4/C materials, J. Power Sources. 160 (2006) 570–576. https://doi.org/10.1016/j.jpowsour.2006.01.042.

[28] Y. Lin, M.X. Gao, D. Zhu, Y.F. Liu, H.G. Pan, Effects of carbon coating and iron phosphides on the electrochemical properties of $LiFePO_4$/C, J. Power Sources. 184 (2008) 444–448. https://doi.org/10.1016/j.jpowsour.2008.03.026.

[29] M.C. Smart, Electrolytes for Low-Temperature Lithium Batteries Based on Ternary Mixtures of Aliphatic Carbonates, J. Electrochem. Soc. 146 (2002) 486. https://doi.org/10.1149/1.1391633.

[30] C. Ho, I.D. Raistrick, R.A. Huggins, Application of A-C Techniques to the Study of Lithium Diffusion in Tungsten Trioxide Thin Films, J. Electrochem. Soc. 127 (1980) 343–350. https://doi.org/10.1149/1.2129668.

[31] B. Levenfeld, M.E. Sotomayor, W. Bucheli, J.-Y. Sanchez, A. Varez, J.M. Amarilla. Electrodes for rechargeable lithium batteries, ES2633149-A1, ES2633149-B2, 2016; WO2017158223-A1 (2017).

[32] A. Aboulaich, R. Bouchet, G. Delaizir, V. Seznec, L. Tortet, M. Morcrette, P. Rozier, J.M. Tarascon, V. Viallet, M. Dollé, A new approach to develop safe all-inorganic monolithic li-ion batteries, Adv. Energy Mater. 1 (2011) 179–183.

https://doi.org/10.1002/aenm.201000050.

Table 1

Power law index (n) and activation energy (E_a) of LFP/C feedstocks with different powder loadings. The linear regression coefficients associated to the fitting are given between brackets.

Powder loading (vol. %)	**n**				**E_a (kJ mol^{-1})**
	160 °C	170 °C	180 °C	190 °C	
50	0.35 (0.997)	0.34 (0.9997)	0.30 (0.9990)	0.30 (0.9994)	11.2
52.5	0.33 (0.994)	0.31 (0.991)	0.29 (0.98)	0.28 (0.9999)	20.0
55	0.29 (0.996)	0.25 (0.993)	0.22 (0.996)	0.22 (0.991)	33.1
58	0.29 (0.993)	0.26 (0.993)	0.24 (0.996)	0.22 (0.992)	33.1

Figure 1
Click here to download high resolution image

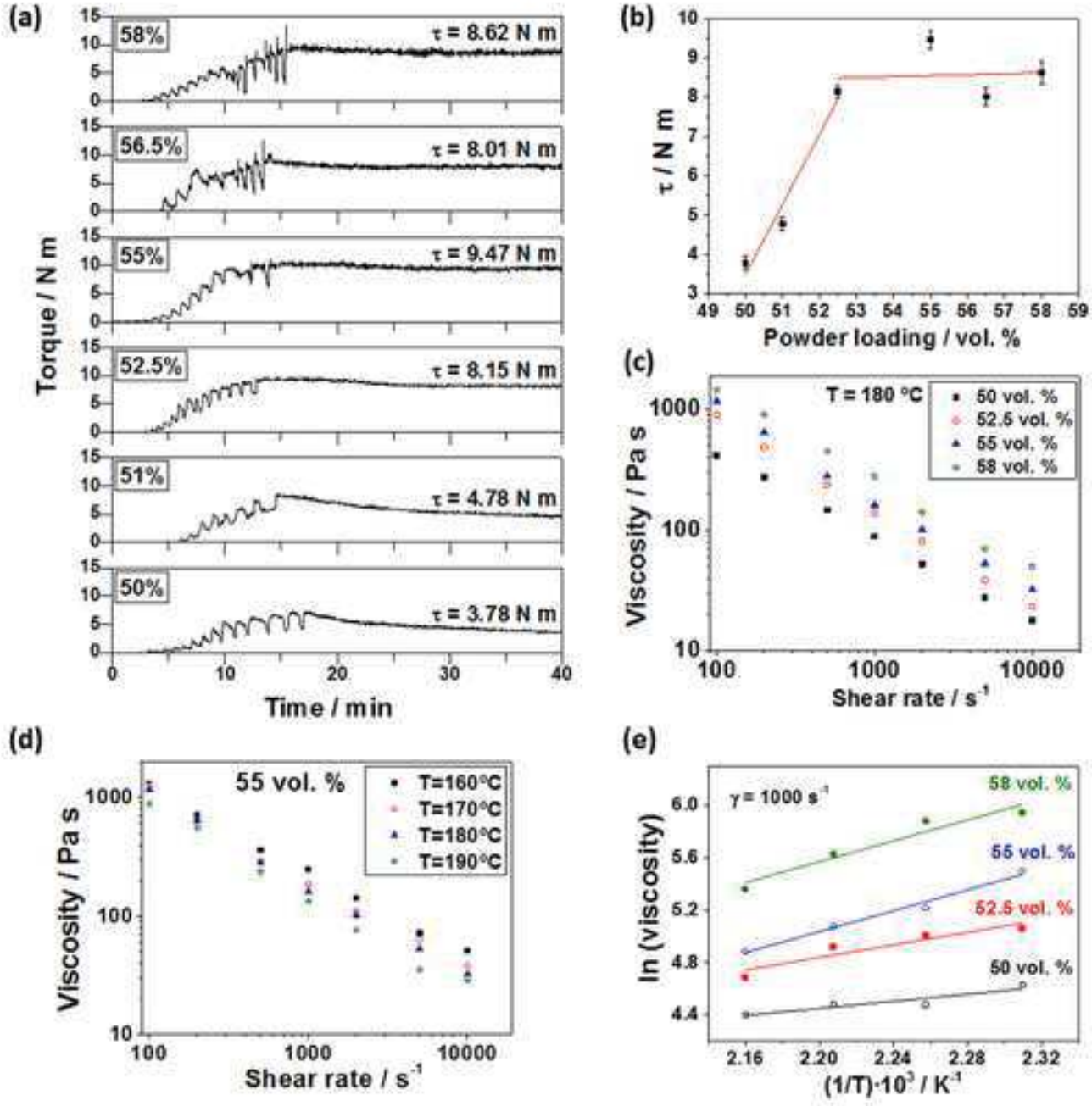

Figure 2

Click here to download high resolution image

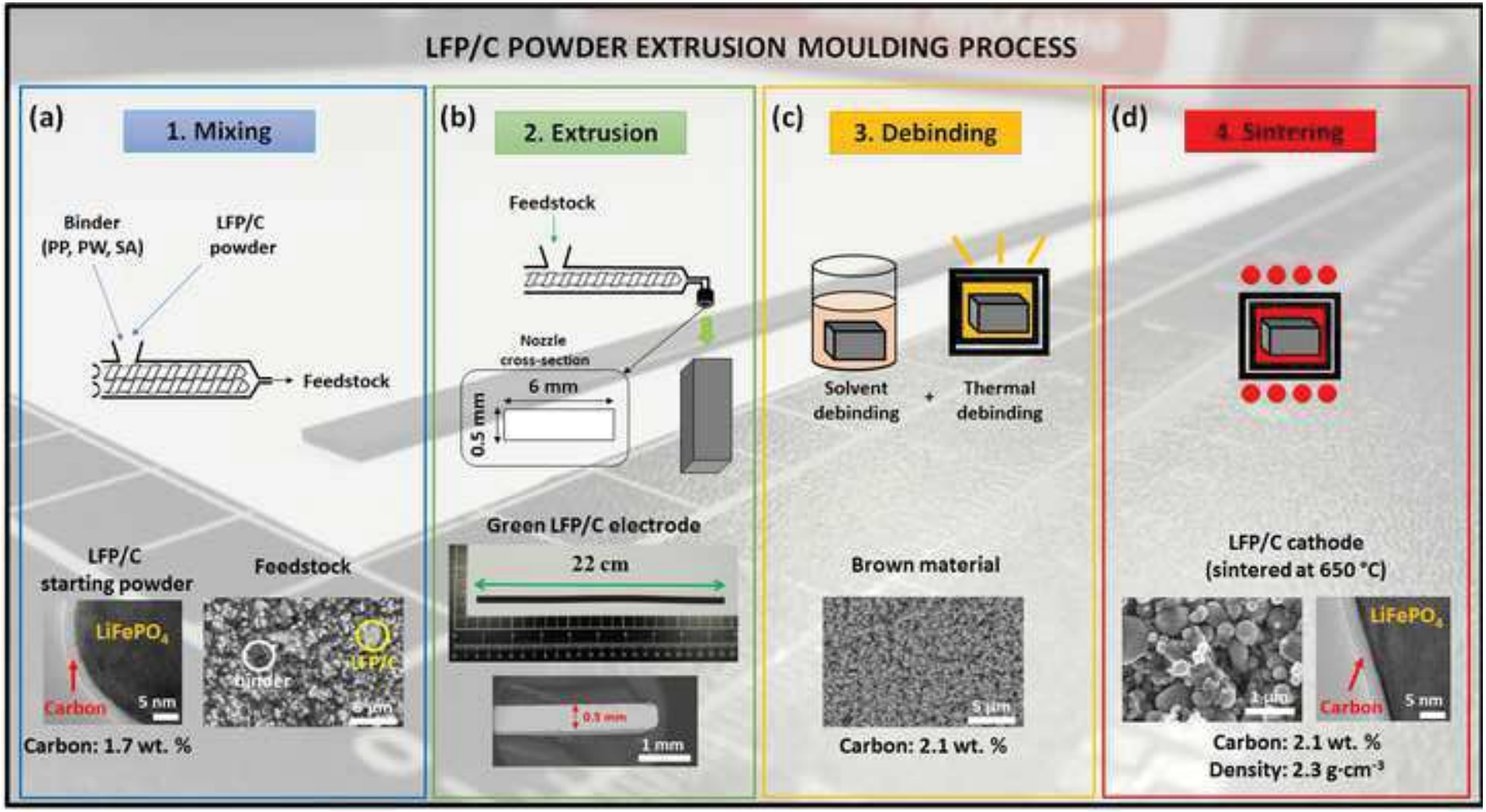

Figure 3 new

Click here to download high resolution image

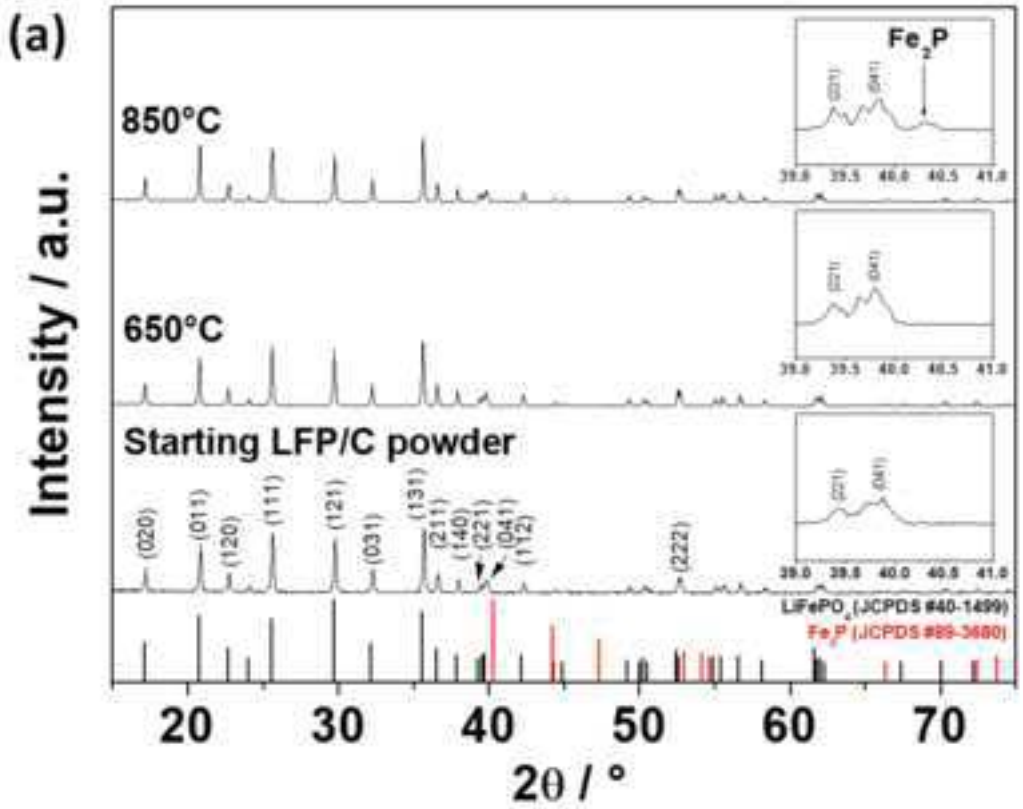

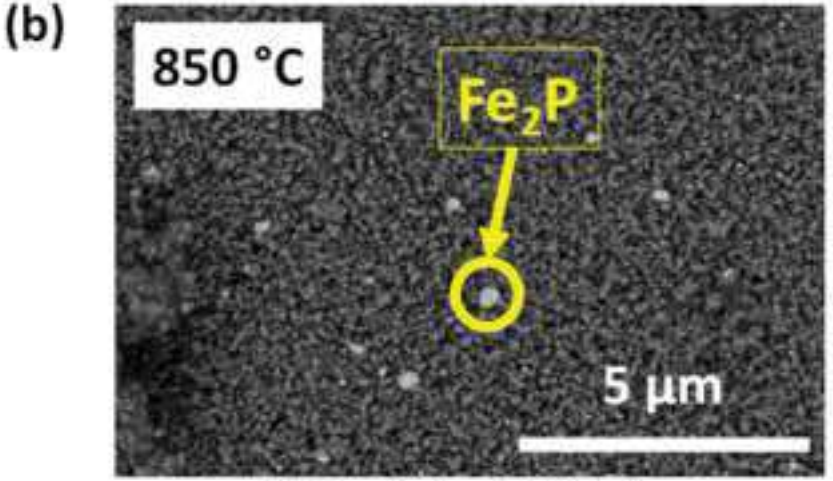

EDS analysis of Fe_2P phase

Element	wt. %	at. %
O K	4.7	12.8
P K	21.1	29.5
Fe K	74.2	57.7

Figure 4
Click here to download high resolution image

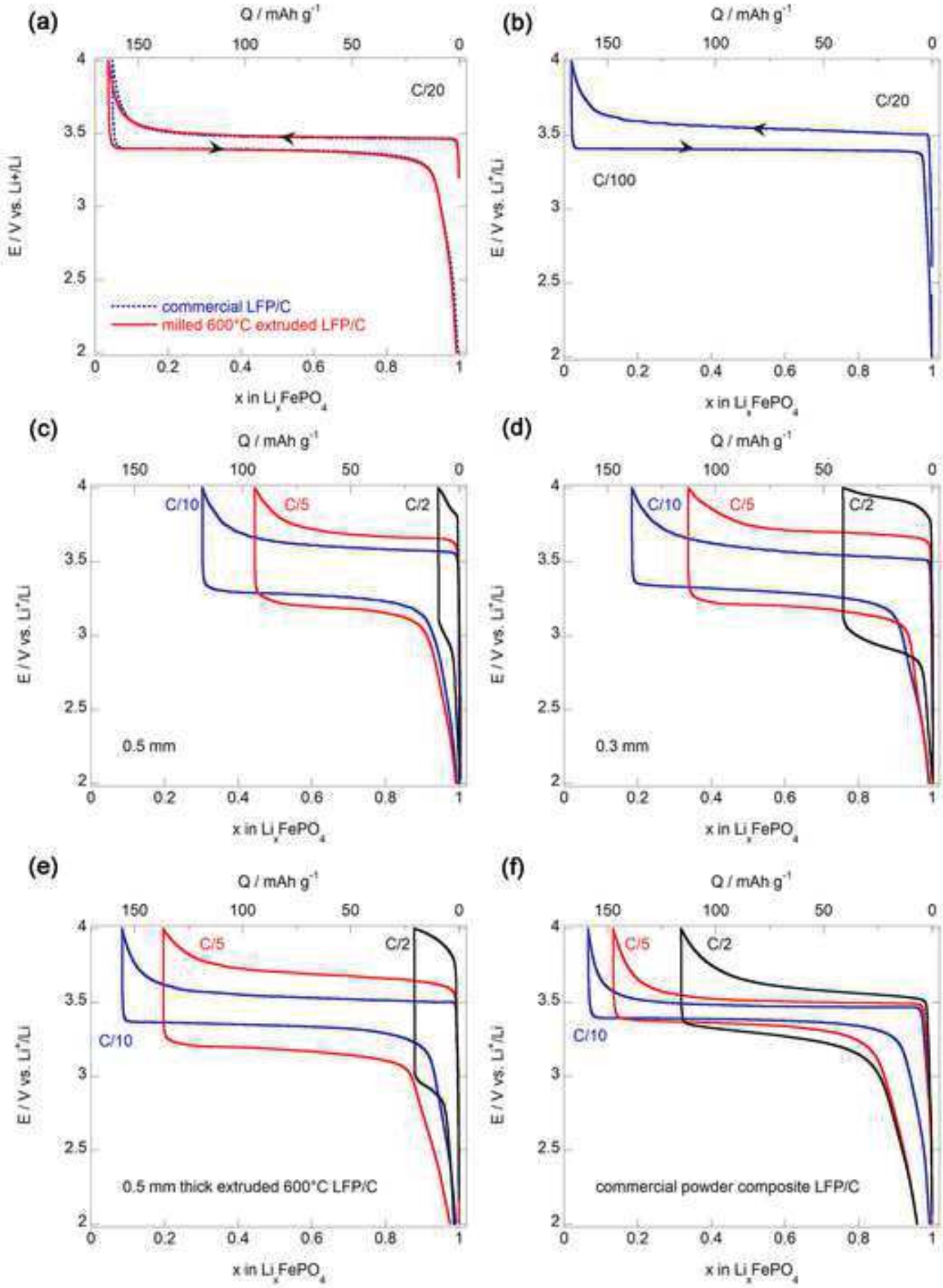

Figure 5
Click here to download high resolution image

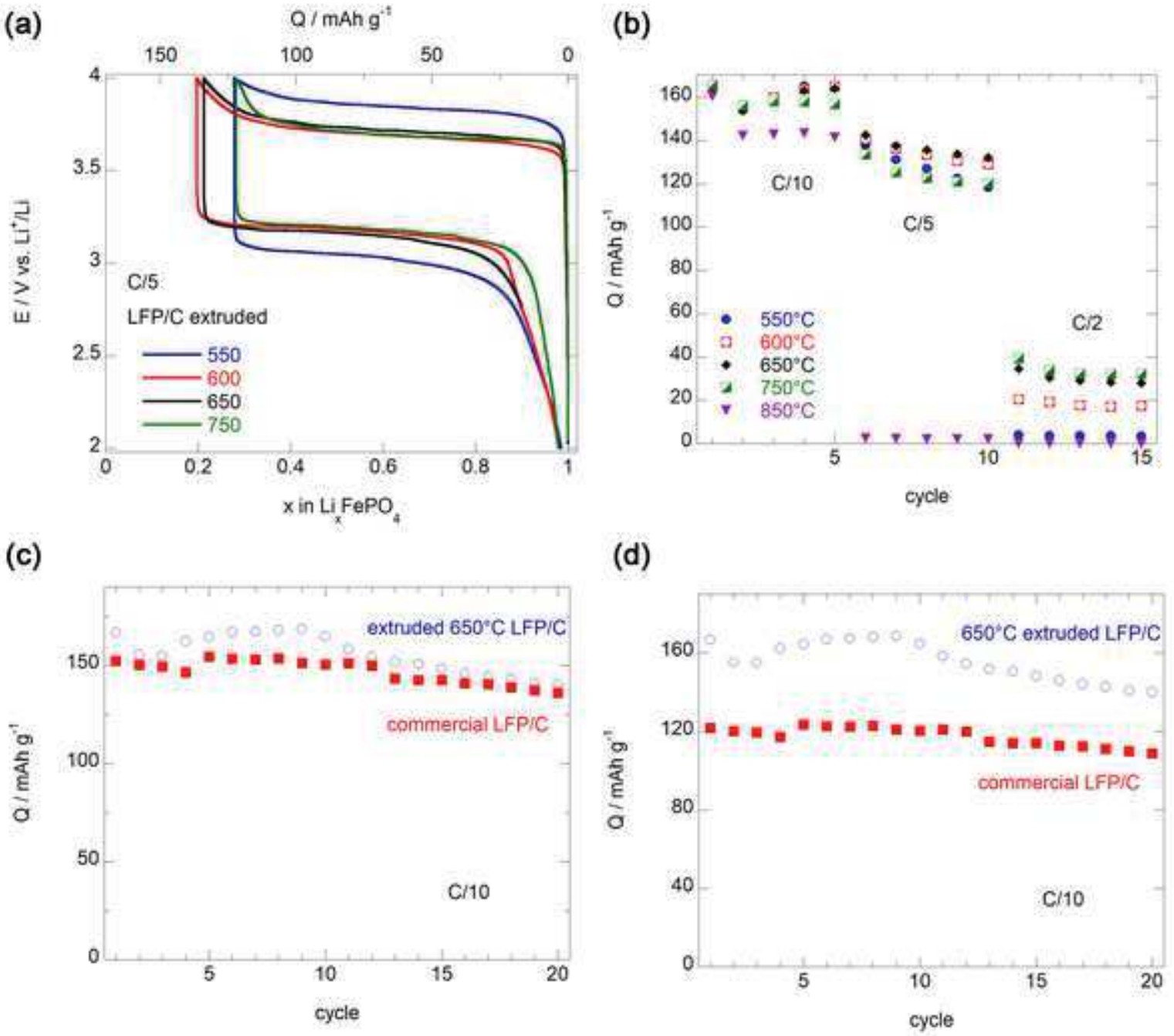

Figure 6
Click here to download high resolution image

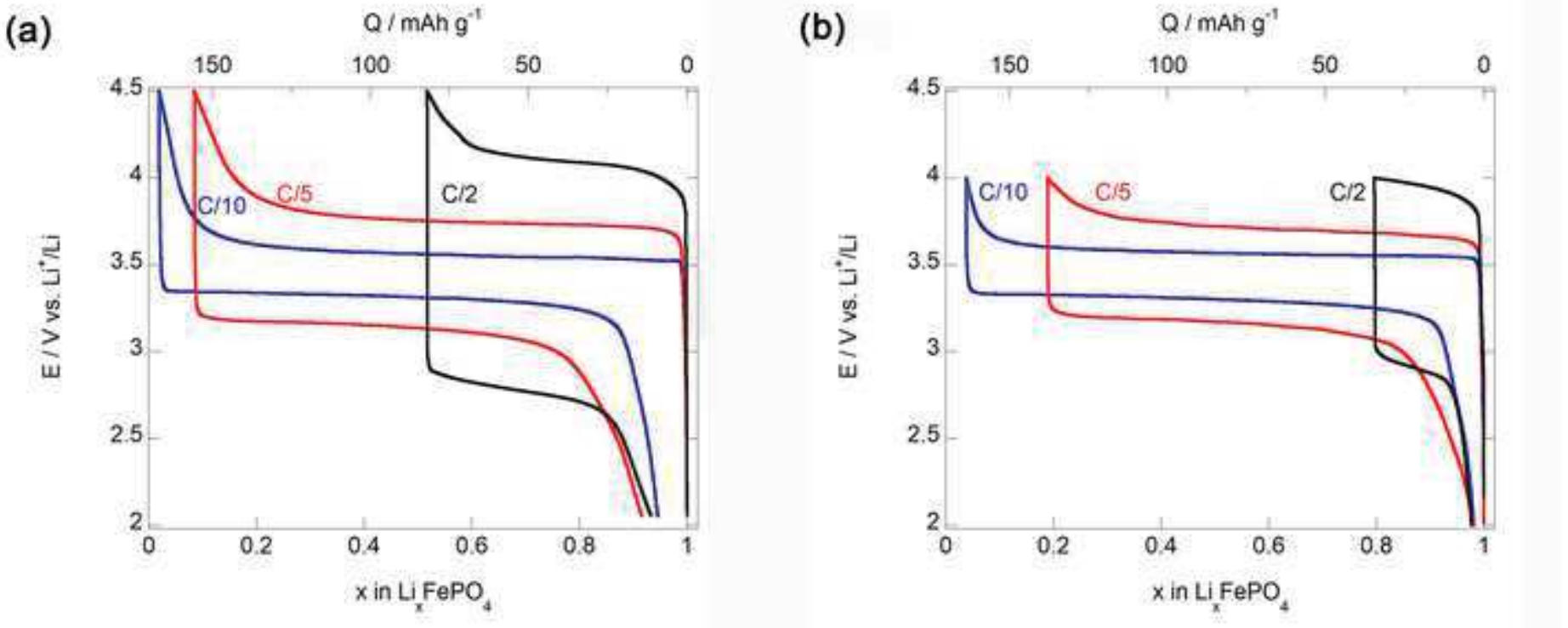

Figure 7

Click here to download high resolution image

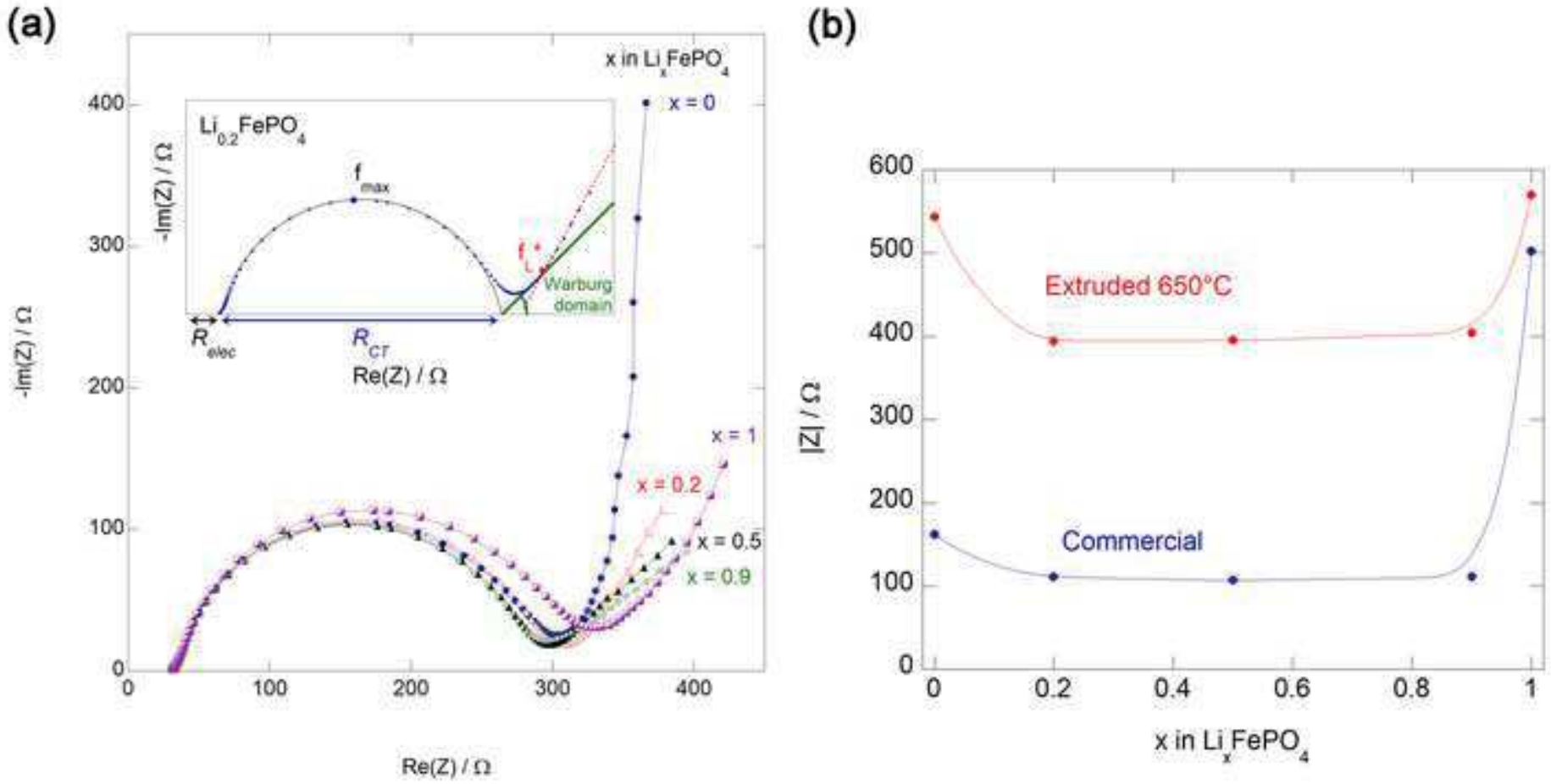

Supplementary Materials

Click here to download Supplementary Materials: Supplementary information_ 10-02-20.pdf

***Credit Author Statement**

Carmen de la Torre-Gamarra: Investigation, Writing - Original Draft, Visualization

María Eugenia Sotomayor: Investigation, Writing - Original Draft

Jean-Yves Sanchez, Supervision

Belén Levenfeld, Writing - Review & Editing, Funding acquisition

Alejandro Várez, Writing - Review & Editing, Funding acquisition, Supervision

Barbara Läik: Investigation, Writing - Original Draft, Visualization

Jean-Pierre Pereira-Ramos: Writing - Original Draft, Supervision

***Declaration of Interest Statement**

Declaration of interests

☒ The authors declare that they have no known competing financial interests or personal relationships that could have appeared to influence the work reported in this paper.

☐The authors declare the following financial interests/personal relationships which may be considered as potential competing interests: